



Delft University of Technology

## A meso-scale model toward concrete water permeability regarding aggregate permeability

Liang, Minfei; Feng, Kun; He, Chuan; Li, Yuqiang; An, Lin; Guo, Wenqi

**DOI**

[10.1016/j.conbuildmat.2020.120547](https://doi.org/10.1016/j.conbuildmat.2020.120547)

**Publication date**

2020

**Document Version**

Final published version

**Published in**

Construction and Building Materials

**Citation (APA)**

Liang, M., Feng, K., He, C., Li, Y., An, L., & Guo, W. (2020). A meso-scale model toward concrete water permeability regarding aggregate permeability. *Construction and Building Materials*, 261, 1-15. Article 120547. <https://doi.org/10.1016/j.conbuildmat.2020.120547>

**Important note**

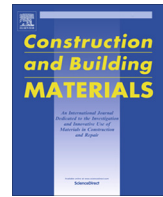
To cite this publication, please use the final published version (if applicable).  
Please check the document version above.

**Copyright**

Other than for strictly personal use, it is not permitted to download, forward or distribute the text or part of it, without the consent of the author(s) and/or copyright holder(s), unless the work is under an open content license such as Creative Commons.

**Takedown policy**

Please contact us and provide details if you believe this document breaches copyrights.  
We will remove access to the work immediately and investigate your claim.



## A meso-scale model toward concrete water permeability regarding aggregate permeability



Minfei Liang <sup>a,c</sup>, Kun Feng <sup>a,\*</sup>, Chuan He <sup>a</sup>, Yuqiang Li <sup>a</sup>, Lin An <sup>b</sup>, Wenqi Guo <sup>a</sup>

<sup>a</sup> Key Laboratory of Transportation Tunnel Engineering, Ministry of Education, Southwest Jiaotong University, Chengdu, China

<sup>b</sup> Department of Civil and Earth Resources Engineering, Kyoto University, Kyoto, Japan

<sup>c</sup> Faculty of Civil Engineering and Geosciences, Delft University of Technology, Delft, The Netherlands

### HIGHLIGHTS

- A sophisticated meso-scale model was developed using an efficient algorithm.
- The effect of aggregate permeability on concrete water permeability is illustrated and estimated.
- The importance of aggregate permeability is illustrated for precise meso-scale model.

### ARTICLE INFO

#### Article history:

Received 9 January 2020

Received in revised form 26 July 2020

Accepted 12 August 2020

Available online 26 August 2020

#### Keywords:

Concrete water permeability

Aggregate

Permeation experiment

Numerical simulation

Meso-scale model

### ABSTRACT

The permeability of natural aggregate is close to cement mortar with relative lower w/c ratios, therefore when calculating the overall concrete water permeability, the effect of aggregate permeability cannot be neglected. This paper presents a sophisticated 3D three phase meso-scale model based on an efficient method of generating random ellipsoidal particles within confined cylindrical space. The meso-scale model considers concrete as the combination of mortar, aggregate and interfacial transition zone, and is used to characterize the permeability of concrete. Furthermore, a series of permeation experiments of concrete with different w/c ratios and aggregate volume fractions are conducted to exemplify the effects of aggregates on concrete water permeability and provide parameters and verification for numerical models. The effects of aggregate permeability on concrete water permeability is evaluated based on both experimental and numerical results. And the permeability coefficient of aggregate adopted in the experiment is estimated reasonably and incorporated into further numerical predictions of concrete water permeability. By comparing the experimental and numerical results, the applicability of meso-scale model proposed here is validated and the effects of aggregate on water permeability of concrete with different w/c ratios vary from each other, depending on the ratio of water permeability of aggregate and mortar.

© 2020 Elsevier Ltd. All rights reserved.

### 1. Introduction

Concrete is a typical permeable porous material, whose permeability highly depends on its porosity and pore structure. For concrete structures under high water pressure (i.e. bridges, subsea tunnels, dams), water permeates into concrete under the action of pressure gradient, during which water not only act as the main agent causing the deterioration of concrete, but also the transport medium for aggressive substance like sulfate or chloride ions [1–4]. Therefore, concrete water permeability is closely related to

the durability of marine structures and should be deeply investigated.

As a straightforward and reliable methodology, physical experiments have been conducted for studying how different constituents of concrete proportion mix affect concrete water permeability [5–13]. Through these experiments, some variables are proved to have significant influence on concrete water permeability, such as water-cement ratio [5–9], aggregate content, size and gradation [6–12], cementitious material types [13], etc. Although physical experiments can get the concrete water permeability directly and precisely, there are still several inherent drawbacks such as difficulties of separating different variables, inefficiency resulting from low permeability of concrete and complexity of experimental procedures [9].

\* Corresponding author.

E-mail address: [windfeng813@163.com](mailto:windfeng813@163.com) (K. Feng).

Due to the random distribution of aggregates, concrete possesses a highly heterogenous meso-structure which is composed of aggregate, mortar and interfacial transition zone (ITZ). Because the influences of meso-structure are impractical to quantify from physical experiments alone, various numerical meso-scale models have been widely adopted to investigate and predict the transport properties of concrete. Recently, many researchers have concentrated on the study of concrete chloride diffusivity. Du et al. [14] developed a 2D three-phase meso-scale model to study the chloride diffusivity of concrete, concluding that aggregate content, ITZ and water-cement ratio have significant influence while aggregate shape and distribution make no difference in diffusivity of concrete. Similarly, Liu et al. [15] concluded that aggregate shape has little impact when it has lower tortuosity based on a series of 2D meso-scale models with different shapes of aggregates. However, based on 3D meso-scale models and experiments, other researches [16–19] have indicated that different aggregate shapes produce different chloride diffusivity: Using ellipsoidal aggregate of different aspect ratios, Zheng et al. [16] and S.D. Abyaneh et al. [17] concluded that the larger the aggregate aspect ratio, the smaller the chloride diffusivity of concrete. Wang et al. [18] conducted in-door experiments and numerical modeling, indicating that different aggregate size lead to different concrete chloride diffusivity. Wu et al. [19] attached high significance to the influence of aggregate shape on concrete chloride diffusivity through meso-scale modeling and experiments. Apart from aggregate, components ranging from ITZ properties [14,15,17,18], water-cement ratio [14,17] to degree of hydration [17] were also investigated and evaluated.

Meanwhile, meso-scale modeling were also employed to quantify the influence of meso-structure parameters on water permeability, which is another important indication of concrete durability. Zhou et al. [20] employed a 2D three-phase mesoscale model and statistical analysis to investigate concrete water permeability. Wimalasiri et al. [21] developed a 2D meso-scale model to simulate permeability degradation of concrete, concluding that the permeability of concrete starts to increase when the applied stress in concrete reaches a certain threshold value for the given aggregate fraction. However, 2D modeling has inherent limit such as insufficient consideration of aggregate spatial effect, which could cause the stimulation results less accurate. Accordingly, Xinxin Li et al. [22,23] proposed a 3D mesoscale model, in which concrete was considered as a heterogeneous three-phase composites, consisting of homogeneous mortar, impermeable aggregate and ITZs. Based on the model, the influence of aggregate (i.e. content, gradation, shape), ITZs (i.e. thickness and permeability) and representative volume element was investigated. Subsequently, Chun-QING Li [24] extended the meso-scale model to a probabilistic investigation, indicating that hydraulic conductivity and thickness of the ITZ are the most influential factors affecting the bulk hydraulic conductivity of concrete. However, based on the assumption that aggregates possess denser microstructure than mortar, the aforementioned researches [14–24] simplified the aggregate as impermeable. While in fact, as the widely employment of High Strength Concrete with relatively low water/cement ratio, the assumptions have become more and more impractical to predict the transport properties of modern concrete. Moreover, the effects of aggregate shape on concrete water permeability were mostly based on a 2D modeling or assuming the shape of aggregates as spheres [20–24], which is inadequate for a deeper understanding.

In this paper, a sophisticated 3D three phase meso-scale concrete model composed of ellipsoidal particles, thin shells and homogeneous matrix is generated. Using FEM, water permeability of concrete is calculated by exerting a steady flow through its

meso-structure. Accordingly, physical experiments with 4 sets of water-cement ratios and 6 sets of aggregate volume fractions are conducted to exemplify the effects of aggregates on concrete water permeability. Then, based on the numerical modeling and experimental results, the permeability of aggregate is estimated reasonably and incorporated into further numerical investigation of concrete water permeability. Finally, the numerical results are validated by experimental results, which proves that the proposed meso-scale model is an efficient and reliable way to predict the water transport behavior in concrete.

## 2. The exemplification of natural permeable aggregate

In previous studies, aggregate is roughly simplified as impermeable because of presuming denser micro-structure, so many studies concluded that higher aggregate content can result in lower concrete water permeability. However, as is shown in Fig. 1, referring to studies concerning water permeability of different intact rocks and concrete of different w/c ratio, permeability coefficient of different natural intact rock is  $1 \times 10^{-15} \sim 1 \times 10^{-10}$  m/s [25–30], while for cement mortar with different w/c ratio, it varies from  $1 \times 10^{-15}$  m/s to  $1 \times 10^{-9}$  m/s [4,9,31,32], which has no obvious difference with the former one. Generally, the rocks used in concrete as coarse aggregates, which often derived from rivers or mountains, are mainly composed of granite and limestone. As is shown in Fig. 1, the permeability coefficient of granite and limestone are approximately in the range of  $1 \times 10^{-10} \sim 1 \times 10^{-15}$  m/s, which is almost coincident with that of cement mortar whose w/c ratio lower than 0.5. Therefore, the assumption that aggregate is far more impermeable than cement mortar seems more untenable when the w/c ratio is lower than 0.5. Besides, for recycled aggregates, the permeability coefficient is much greater than that of natural aggregate and can lead to a totally opposed conclusion against previous studies. Therefore, the assumption that aggregate is impermeable is likely to result in unwanted errors when it comes to practice.

In order to derive more precise predictive value of concrete water permeability, it's important to figure out the relationship between the permeability of cement mortar and aggregate. In other words, the key is to find out the permeability ratio of aggregate to cement. However, the aggregate permeability can hardly be tested precisely because of irregular shape. Moreover, for aggregate derived from the same region, the range of aggregate permeability may be precise to some extent, but a very precise value is hard to get because of inherent variance in constituent minerals. Therefore, it's impractical to incorporate aggregate of certain water permeability in permeation test. In order to consider the influence of different permeability ratio of aggregate to cement mortar, by adopting one kind of natural aggregate and different w/c ratios, a series of experiments containing different permeability ratio of aggregate to cement mortar are conducted to provide parameters and verification for numerical models. With the experimental results, the meso-scale numerical model is established to estimate the aggregate permeability, which is used in further numerical model of concrete water permeability and verified by experimental results.

## 3. Meso-scale modeling

In order to quantitatively study the permeable characteristics of concrete which is affected greatly by content, permeability and shape of aggregate, a three phase meso-scale model composed of aggregate, mortar and ITZ is established. Assuming the permeation of concrete obeys Darcy's law, the transport equations in the permeation field are formulated and solved using FEM, in which the

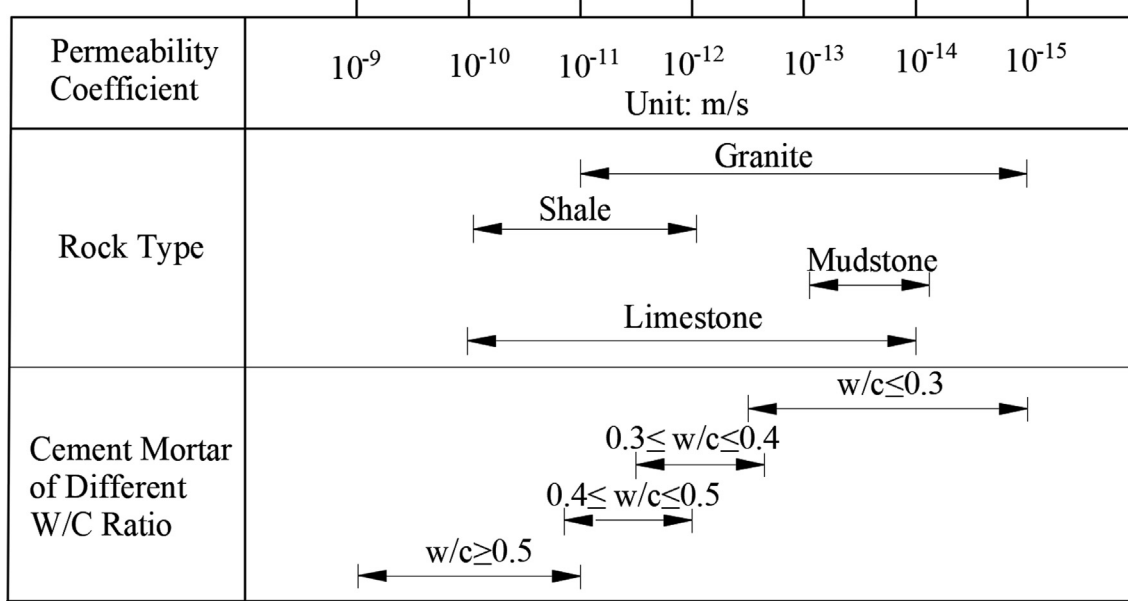


Fig. 1. Range of Water permeability coefficient of Different Types of Rocks and Concrete.

three components are meshed separately and the continuity of fluxes at ITZ is applied. In the model, each phase (i.e. mortar, aggregate and ITZ) is considered as homogeneous constituent and will be assigned with different parameters. As important parameters of this model, the permeability coefficient of mortar, aggregate, ITZ and concrete will be represented by  $k_m$ ,  $k_a$ ,  $k_i$ ,  $k_{eff}$ , respectively. The  $k_m$  is obtained directly from the experimental results and the value of  $k_i$  will be derived through previous studies and parametric calculation. Finally, the value of  $k_a$  will be estimated reasonably and further incorporated in numerical model to be verified by experimental results.

### 3.1. Random ellipsoidal aggregate model

A 3D random ellipsoidal aggregate structure is developed to stimulate the concrete specimen, which use rounded gravel of certain sizes and exact volume fractions as aggregates.

#### 3.1.1. Size distribution of aggregates

The aggregate volume fractions are set to be 0–50%, and the size are confined to 5–10 mm and 10–25 mm. The distribution of aggregates obeys the Fuller curve [33], which can be written as:

$$P(D) = \left( \frac{D}{D_{\max}} \right)^0.5 \quad (1)$$

In Eq. (1), D is the grain diameter of aggregate;  $D_{\max}$  is the maximum grain diameter;  $P(D)$  is the mass ratio of aggregates whose grain diameter is smaller than D to overall aggregates. The distribution pattern of sizes and positions of aggregates is set to obey the continuous uniform distribution function, which is a common distribution function in Theory of Probability.

In order to quantify the effects of ellipsoidal aggregates, widely used parameters termed as ‘aspect ratio’ and ‘flatness ratio’ are adopted here [16,17,34]. According to statistical results of natural gravel aggregates [34], the aspect ratio and flatness ratio is set to be 1 ~ 2 and 1 ~ 1.6, respectively, as is shown in Eqs. (2a) and (2b).

$$1 \leq \beta_1 = \frac{r_a}{r_b} \leq 2 \quad (2a)$$

$$1 \leq \beta_2 = \frac{r_b}{r_c} \leq 1.6 \quad (2b)$$

In Eq. (2),  $\beta_1$ ,  $\beta_2$  is the aspect ratio and flatness ratio;  $r_a$ ,  $r_b$ ,  $r_c$  is length of the longest, intermediate and shortest axis of ellipsoidal aggregate.

#### 3.1.2. Mathematical expression for spatial ellipsoidal aggregates

In order to stimulate random rounded gravel aggregate, the spatial characteristics of ellipsoidal particle (i.e. lengths, orientations of axes and center coordinates) are expressed by a quadratic matrix. The generation of random aggregate structure is performed in two steps: Firstly, a standard ellipse with its center fixed at (0,0,0) and axes paralleled to the Cartesian axes is generated. Then, a translation and rotation matrix is generated randomly to transform the ellipse’s position and orientation.

According to Fuller curve mentioned above, lengths of ellipsoidal axes ( $r_a$ ,  $r_b$ ,  $r_c$ ) are randomly generated. Then the quadratic matrix of a standard ellipse can be written as:

$$A_0 = \begin{pmatrix} 1/r_a^2 & & & \\ & 1/r_b^2 & & \\ & & 1/r_c^2 & \\ & & & -1 \end{pmatrix} \quad (3)$$

With the axis length of aggregates settled, the axis orientations and center coordinates are randomly generated and then form a translation and rotation matrix written as:

$$T = \begin{pmatrix} \cos a_x & \cos b_x & \cos c_x & x_c \\ \cos a_y & \cos b_y & \cos c_y & y_c \\ \cos a_z & \cos b_z & \cos c_z & z_c \\ 0 & 0 & 0 & -1 \end{pmatrix} \quad (4)$$

where  $x_c$ ,  $y_c$ ,  $z_c$  represent the center coordinates;  $a_x$ ,  $a_y$ ,  $a_z$ ;  $b_x$ ,  $b_y$ ,  $b_z$ ;  $c_x$ ,  $c_y$ ,  $c_z$  represent for the angles between the ellipsoidal axes and Cartesian axes. Subsequently, the quadratic matrix of random ellipsoidal particle can be expressed as:

$$A = (T^{-1})^T A_0 T \quad (5)$$

#### 3.1.3. Overlap detection between ellipsoidal aggregates

In order to prevent randomly generated aggregates from overlapping, the algebraic method proposed by Wang et al. [35] is

adopted here: For two ellipsoids whose quadratic matrix are  $A_1$  and  $A_2$ , respectively, they are separated only if the characteristic equation  $\det(\lambda \times A_1 + A_2) = 0$  has two distinct roots.

Generally, coarse aggregates take up 40–50% of concrete volume [36], so the overlap of random aggregates is very likely to happen, which means masses of computation if the algebraic method above is performed endlessly. In that case, a simpler algebraic method is adopted firstly: only if the distance between two ellipsoidal centers (assigned to  $d$ ) satisfy the algebraic condition of  $r_{c1} + r_{c2} < d < r_{a1} + r_{a2}$ , is Wang's method [35] necessary to be performed, or the relationship between the two ellipsoidal can be determined as separated or overlap.

### 3.1.4. Aggregate packing procedure

Although the mathematical expression of aggregate and overlap detection are settled, it's still very time-consuming to pack hundreds of particles with random size, position and orientation in a confined cylindrical space. Hereby, based on an efficient method termed as 'Removal and Occupation method' [37], an improved node local density-oriented packing method is adopted here.

As is shown in Fig. 2, the cylindrical packing space is discretized into finite number of nodes, which are stored into a matrix termed as  $S$  and used as the center points of random aggregates. Every time an aggregate is generated successfully, the nodes it occupied will be removed from  $S$ . Specifically, the identification of occupied nodes can be based on the ellipsoidal quadratic matrix  $A$  (shown in Eq. (5)): for a node located at  $(x_c, y_c, z_c)$ , if  $X^TAX > 0$  (where  $X = \{x_c, y_c, z_c, 1\}$ ), the node is outside the aggregate, else the node is inside the aggregate and should be removed from  $S$ . By this way, the size of  $S$  keeps shrinking as the packing procedure going on.

After hundreds of times of random packing (e.g. 20% of aggregate are finished), however, most nodes remained are extremely scattered by random ellipsoidal aggregates and are hard to pack any other aggregates. Accordingly, a node local density-oriented method is proposed here, which helps to find a series of evenly distributed nodes to place the aggregate properly. As is shown in Fig. 3, the process of node local density-oriented method goes as follows:

- (1) Firstly, an initial node  $n_0$  is randomly picked from node matrix  $S$ .

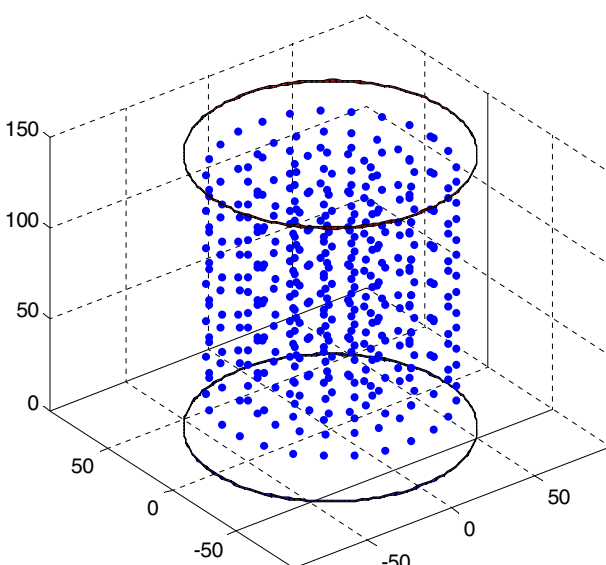


Fig. 2. The discretization of packing space.

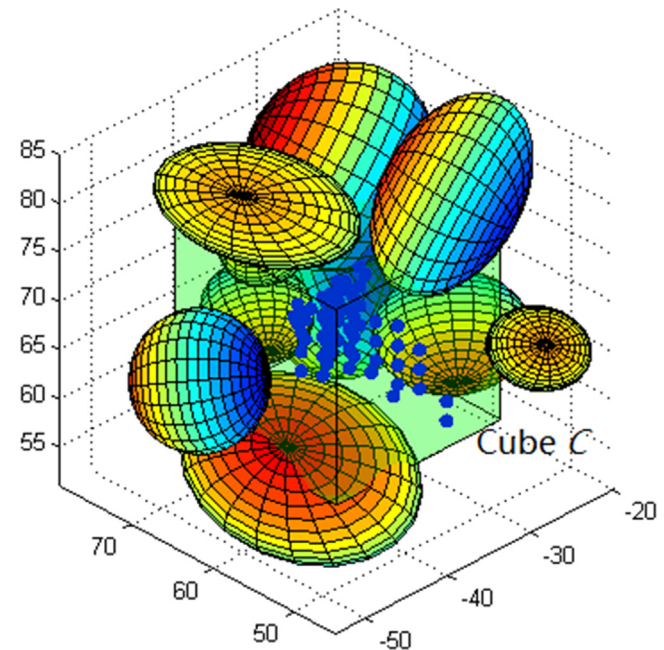


Fig. 3. Node Local Density-Oriented Method.

- (2) Then, use the node  $n_0$  as the center of a cube  $C$  whose side length is determined as double the length of the aggregate's first axis  $r_a$ .
- (3) Finally, the number of nodes that located inside the cube  $C$  (set as  $N_1$ ) is calculated. If the value of  $N_1$  is bigger than the required minimum number of nodes  $N_{min}$ , then we can presume that the nodes in cube  $C$  are highly probable to place the aggregate properly and are stored into matrix  $S_1$ .

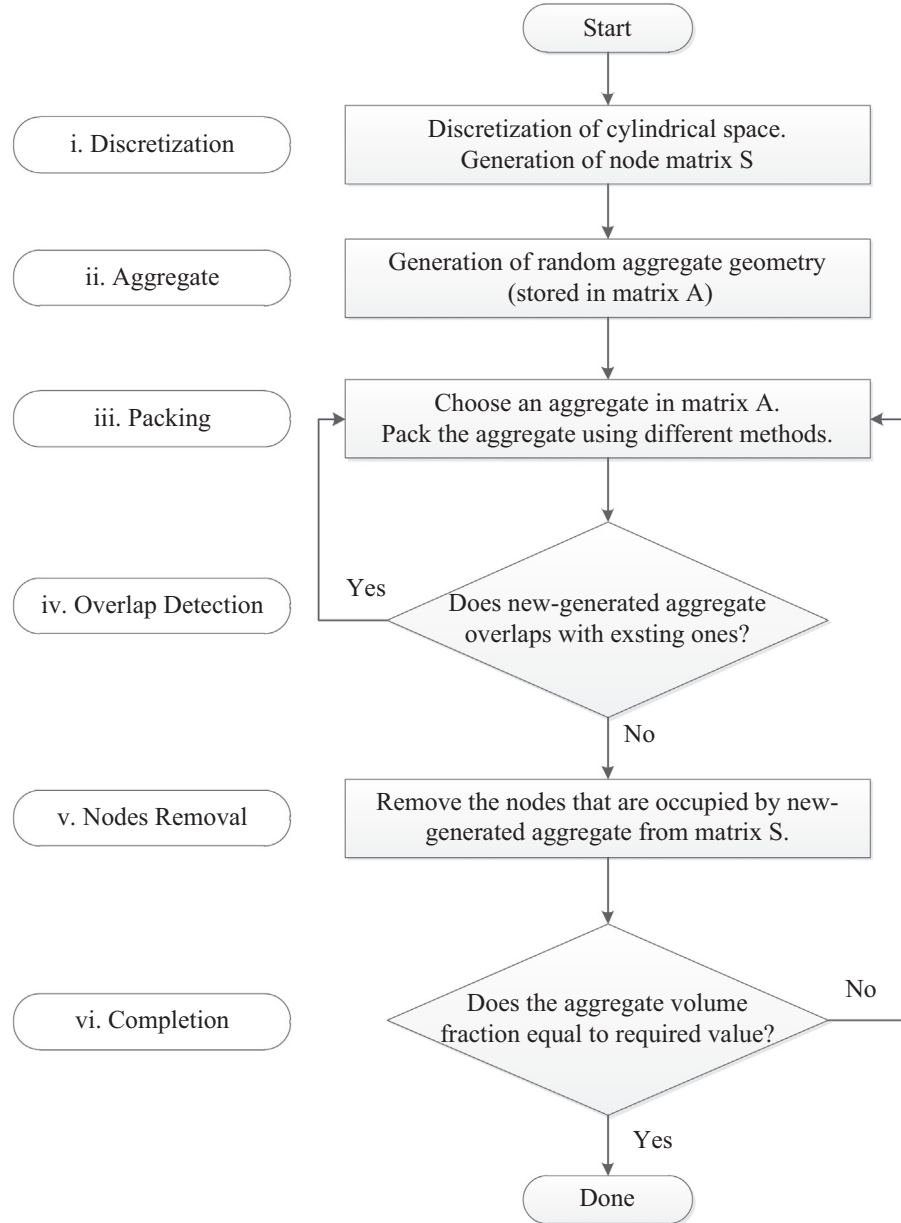
The value of  $N_{min}$  is significant for this process. Based on the fact that the nodes are distributed densely and deleted continuously in every packing iteration, it can assume that the nodes inside cube  $C$  distributed continuously. Thereafter, the enveloping volume of nodes is proportional to the number of nodes and can be easily calculated according to the original density of nodes. When the enveloping volume of nodes inside cube  $C$  is equal to the volume of aggregate, then the nodes in cube  $C$  can be highly probable to place the aggregate properly. Therefore, the value of  $N_{min}$  can be determined and expressed as:

$$N_{min} = \frac{4\pi^2 R^2 h r_a r_b r_c}{3N_0} \quad (6)$$

where  $R$  (L),  $h$  (L) represents the radius and height of concrete specimen.  $N_0$  is the initial number of nodes in first iteration of aggregate packing procedure.

The generation process of random aggregate structure (shown in Fig. 4) goes as following steps:

- i. Discretize the packing space with a size smaller than that of minimum aggregate, storing the coordinates of mesh nodes in a matrix  $S$ .
- ii. The size and orientation of aggregates are generated randomly according to a uniform probability distribution and stored in a matrix  $A$  in the order of largest to smallest in size.
- iii. For the aggregate ranked top 20% in  $A$ , a node in  $S$  is randomly picked as its center point. For the others, the node local density-oriented method mentioned above is conducted and matrix  $S_1$  is derived, in which a node is randomly picked as the center point of the aggregate.

**Fig. 4.** Generating process of random aggregate structure.

- iv. The new-generated aggregate is detected if it's overlapped or separated with others.
- v. If the new aggregate is separated with others, its geometry will be stored in matrix E and the nodes it has occupied will be removed from S, or step iii ~ v has to be repeated.
- vi. For the next aggregate in A, step iii ~ vi is repeated until the volume fraction of aggregate in E reaches the desired value.

After the steps above, the generation of random aggregate structure is shown in Fig. 5.

### 3.2. FE stimulation of concrete water permeability

#### 3.2.1. Physical field equation

Suppose the concrete skeleton is absolutely rigid and the water flow is incompressible, the continuity equation is obtained. The flow of water in saturated concrete, which is a typical porous medium, obeys Darcy's law and can be written as Eq. (7) [1].

$$\mathbf{v} = -K \nabla h \quad (7)$$

In which  $\mathbf{v}$  ( $\text{LT}^{-1}$ ) is flow velocity,  $K$  ( $\text{LT}^{-1}$ ) is the permeability coefficient,  $h$  ( $\text{L}$ ) is the water head and  $\nabla$  ( $\text{L}^{-1}$ ) is the spatial gradient operator.

As an extreme thin layer between the aggregates and mortars, ITZ (interfacial transition zone) contains higher porosity and more micro-cracks, so it's generally considered as a weak zone inside concrete. Here it's simulated with homogeneous zero-thickness shell element, which is a six-nodes element, of which three nodes are attached to aggregate and mortars, respectively. Compared with solid element, the advantage of zero-thickness shell element is that number of elements are largely reduced so that FEM calculation goes more efficiently. Similar to water flow in fracture of rock mass, water flow in ITZ obeys the tangential form of Darcy's equation [23,38], as is shown in Eq. (8). Note that  $d_i$  here is only a parameter, which is based on the assumption that the thickness of ITZ is uniform. The parameter  $d_i$  is only used in Eq. (8) and will not be modeled in geometry of FEM model.

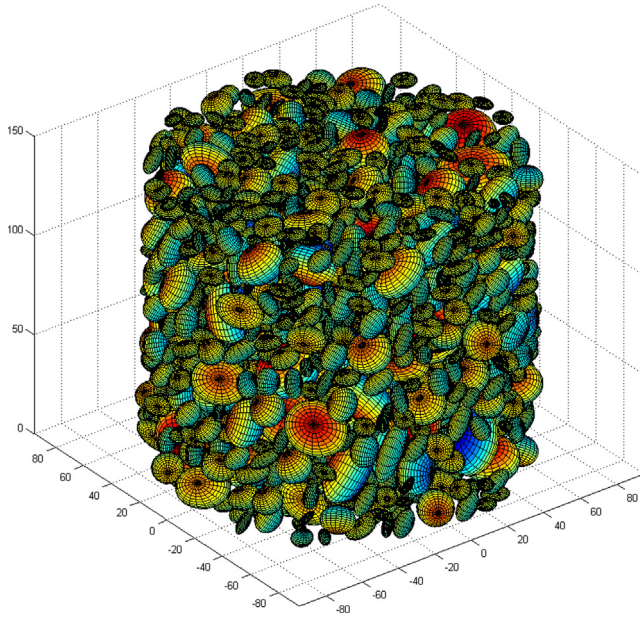


**Fig. 5.** The geometry of random ellipsoidal aggregate structure.

$$Q_i = -K_i d_i \nabla T_i \quad (8)$$

where  $Q_i$  ( $L^2 T^{-1}$ ) is the water flow rate per unit length of ITZ,  $K_i$  ( $LT^{-1}$ ) is the permeability coefficient of ITZ,  $d_i$  ( $L$ ) is the thickness of ITZ,  $\nabla T_i$  ( $L^{-1}$ ) is the gradient operator fixed on the tangential plane of ITZ shell.

### 3.2.2. Meshing and boundary conditions

As is shown in Fig. 6, based on the FE software Comsol Multiphysics, the ITZ shell, mortar body and ellipsoidal aggregate are automatically discretized using triangular and tetrahedral elements, with the maximum size smaller than 2 mm. Meanwhile, according to the configuration of permeation test, the top and bottom of the numerical specimen is subjected to atmospheric pressure and water pressure of 1.2 MPa, and the lateral surface is fixed as non-flux boundary.

### 3.2.3. Derivation of concrete water permeability

Using the FE mesoscale model established here, the distribution of water flow velocity is obtained and used to derive the water permeability of numerical specimen. For instance, when the aggregate volume fraction reaches 40% and w/c is 0.5, the profile of water flow velocity is shown in Fig. 7, in which the effects of tortuosity, dilution and ITZ on water flow velocity inside concrete are well illustrated: Due to the ingress of less permeable aggregate, the effective permeation area is greatly reduced and the tortuous flowline is further lengthened compared to that of non-aggregate mortar. Besides, the ITZs attached on the surface of aggregate bring more weak zones inside concrete, where the flowline tends to be more intensive indicating much greater flow velocity.

Based on the horizontal profile of flow velocity (see Fig. 7(b)), the effective permeability coefficient of concrete water permeability is calculated using Darcy's law:

$$K_{eff} = \frac{\int v dA}{Ai} \quad (9)$$

where  $v$  ( $LT^{-1}$ ) is the flow velocity,  $A$  ( $L^2$ ) is the horizontal section area of specimen,  $i$  is the hydraulic gradient at the selected horizontal section. In order to reduce the variation of  $K_{eff}$  caused by random aggregate structure, statistical analysis are conducted and it shows

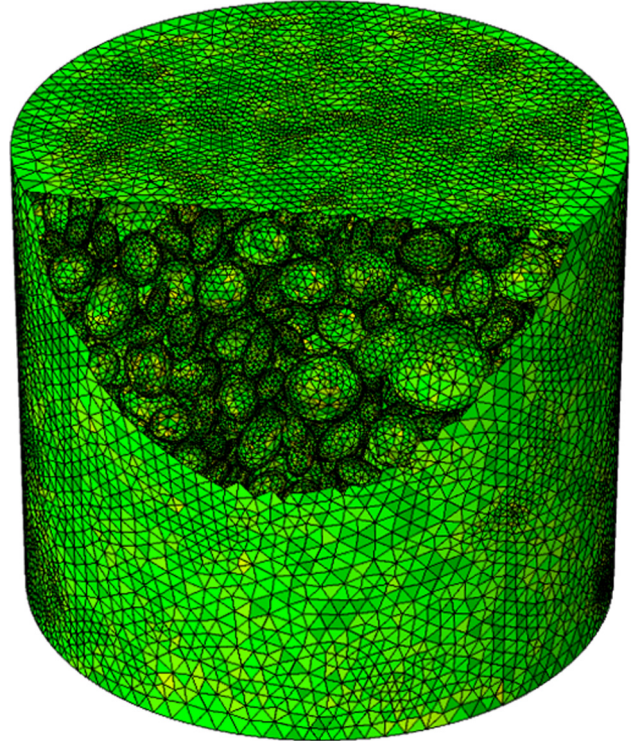


**Fig. 6.** The meshing of numerical model.

that 8 numerical samples are sufficient to confine the variation within 5%.

In the following calculations, the effectiveness factor of concrete water permeability will be adopted as the main measurement. The definition of effectiveness factor of concrete water permeability can be seen in many relative studies [22,23]. Through dividing the concrete water permeability by cement mortar permeability, the effectiveness factor of concrete preclude the influence of cement mortar and is mainly used to illustrate the effects of ITZ or aggregate on concrete water permeability. The effectiveness factor of concrete water permeability can be written as:

$$\eta = \frac{K_{eff}}{k_m} \quad (10)$$

where  $K_{eff}$  ( $LT^{-1}$ ) is the concrete water permeability,  $k_m$  is the water permeability of cement mortar.

### 3.2.4. Derivation of ITZ parameters

As a complex weak zone in concrete, ITZ has drawn many attentions of researchers. Based on various scanning electron microscopic technologies, many studies have observed the shapes and sizes of various ITZs and indicated that the thickness of ITZ (represented by  $d_i$ ) is mostly between 10 ~ 50um [39–42]. With a highly heterogeneous structure, the thickness of largest ITZ can reach 300 um [41]. What's more, the sizes of aggregates have little influence on the thickness of ITZ [43]. According to the studies on permeability of ITZs (represented by  $k_i$ ) considering different w/c ratios and degree of hydration, the permeability coefficient of ITZ (represented by  $k_i$ ) is proved to be 20 ~ 50 times of that of mortar [43,44]. In order for a more precise results of concrete water permeability, a parametric study is conducted here to better understand the effect of ITZ properties. When the value of  $k_i$  is 0 ~ 50 times of  $k_m$  and  $d_i$  is among 0 ~ 300um, the effectiveness factor of concrete water permeability is shown in Fig. 8. Note that the aim of parametric study here is to investigate the effect of ITZ

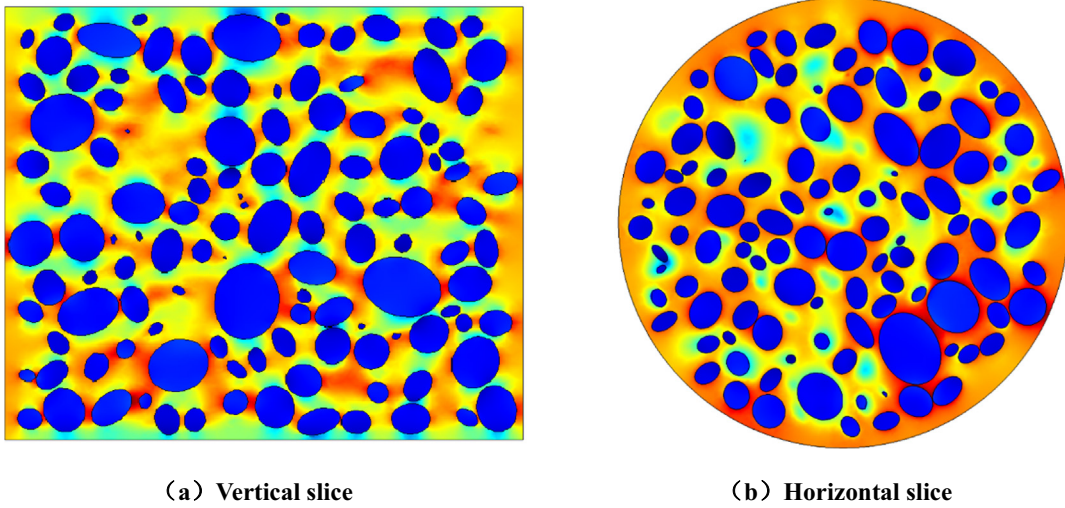


**Fig. 7.** Contour of flow velocity (Unit: m/s).

and does not require high precision of concrete water permeability, so the aggregate adopted here is regarded as impermeable tentatively and a valued of  $10^{-5} \times k_m$  will be assigned to  $k_a$ .

As is shown in Fig. 8, when the value of  $k_i/k_m$  ratio is small ( $k_i/k_m = 2 \sim 10$ ), as the increase of ITZ thickness (represented by  $d_i$ ), the effectiveness factor  $\eta$  increases linearly. While when the value of  $k_i/k_m$  ratio is larger ( $k_i/k_m = 20 \sim 50$ ), although the effectiveness factor  $\eta$  still increases as the ITZ thickness  $d_i$  grows, the growing pattern start to deviate from linear and the slope of  $\eta-d_i$  curve decreases as  $d_i$  increases. When the ITZ thickness  $d_i$  is smaller than 50um or when  $k_i/k_m$  ratio is smaller than 10, the effectiveness factor  $\eta$  is smaller than 1.0, which means that the effects of tortuosity and dilution resulted from impermeable aggregate is the main reason accounting for the concrete water permeability that is lower than cement mortar permeability. While as the increase of  $d_i$  and  $k_i/k_m$  ratio, the effectiveness factor  $\eta$  exceeds 1.0, indicating that the high permeability of ITZ not only offsets the effects of tortuosity and dilution resulted from impermeable aggregate, but as a result increases the overall concrete water permeability. The properties of ITZ are highly depends on not only aggregate, but also w/c ratios and hydration degrees. For the lower w/c ratios, the hydration process stops much earlier since less water is available for further hydration, which result in a higher

value of  $k_i/k_m$  ratio. In order to secure a precise numerical results, based on the reference values that previous studies have recommended [39–44], the existing numerical parametric studies and experimental results (shown in section 3.4), the ITZ thickness  $d_i$  is set to be 20 um, and the  $k_i/k_m$  ratio for w/c = 0.3, 0.4, 0.5, 0.6 is set to be 50, 40, 30, 20, respectively.

### 3.2.5. Effectiveness factor of concrete water permeability

Before effectiveness factor  $\eta$  is used as main measurement for concrete water permeability in the following calculations, a parametric study regarding the effect of  $k_m$  on  $K_{eff}$  is performed to provide better understandings of effectiveness factor  $\eta$ . Based on the most adopted w/c ratios ranging from 0.3 to 0.6, a range of cement mortar water permeability between  $1 \times 10^{-13} \sim 1 \times 10^{-10}$  m/s is adopted in models which possess aggregate fractions of 10%~50% to calculate corresponding concrete water permeability. Note that the calculation here mainly aims at the effect of permeability of mortar matrix. Therefore, the aggregate adopted here is regarded as impermeable tentatively and a value of  $10^{-5} \times k_m$  will be assigned to  $k_a$ . The results is shown in Fig. 9.

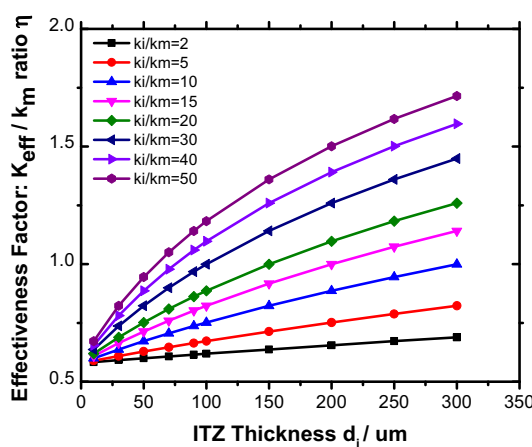


**Fig. 8.** The curve of the permeability coefficient of mortar and the effectiveness factor.

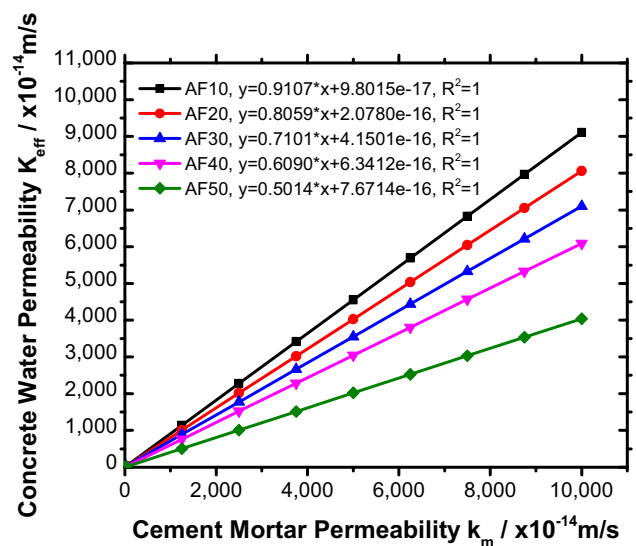


**Fig. 9.** The curve of the permeability coefficient of mortar and concrete water permeability (Note that “AF” represent the aggregate volume fraction).

As is shown in Fig. 9, as the increase of  $k_m$ , the value of  $K_{eff}$  increases linearly. By performing linear fitting on the results of models whose aggregate volume fraction is 10–50%, each correlation coefficient for every model is 1.0. Therefore, for a concrete specimen of certain aggregate volume fraction, a precise linear relationship between  $K_{eff}$  and  $k_m$  can be determined. Moreover, when  $k_m$  approaches 0, the magnitude of  $K_{eff}$  is close to  $10^{-16}$  m/s, which can be almost seen as impermeable. Thereby, the concrete water permeability ( $K_{eff}$ ) is approximately directly proportional to cement mortar permeability ( $k_m$ ), and the slope of  $K_{eff}$  -  $k_m$  curve represent the effectiveness factor of concrete water permeability ( $\eta$ ). For a given aggregate volume fraction and certain ITZ parameters, the effectiveness factor of concrete water permeability ( $\eta$ ) is a fixed constant and is independent from the value of cement mortar permeability ( $k_m$ ).

#### 4. Experimental program

##### 4.1. Materials and mix proportions

As is shown in Table 1, in order to provide parameters and verification for numerical models which contains concrete of different w/c ratios and aggregate volume fractions, 24 types of mix proportions are designed, with the w/c ranging from 0.3 to 0.6 and aggregate volume fraction ranging from 0 to 50%. The design of mix proportions is based on Absolute Volume Method. The P.C 42.5 cement, medium sand and tap water are incorporated as mortar matrix, in which the cement to sand ratios are fixed as 0.3556. Two sizes of approximately ellipsoidal rounded gravels (i.e., 5–10 mm and 10–25 mm, respectively) are used as coarse aggregates (As is shown in Fig. 10). For each mix proportion, 6

**Table 1**  
Experimental mix proportions (kg/m<sup>3</sup>).

No.	w/c	Cement	Sand	Gravel	
				Volume fraction	Amount
1	0.3	586.7	1650.2	0	0
2		528.1	1485.2	10%	266.0
3		469.4	1320.2	20%	532.0
4		410.7	1155.2	30%	798.0
5		352.0	990.1	40%	1064.0
6		293.4	825.1	50%	1330.0
7	0.4	554.2	1558.8	0	0
8		498.8	1402.9	10%	266.0
9		443.4	1247.0	20%	532.0
10		388.0	1091.1	30%	798.0
11		332.5	935.3	40%	1064.0
12		277.1	779.4	50%	1330.0
13	0.5	525.1	1476.9	0	0
14		472.6	1329.2	10%	266.0
15		420.1	1181.5	20%	532.0
16		367.6	1033.8	30%	798.0
17		315.1	886.1	40%	1064.0
18		262.6	738.5	50%	1330.0
19	0.6	498.9	1403.2	0	0
20		399.4	1123.4	10%	266.0
21		299.8	843.1	20%	532.0
22		498.9	1403.2	30%	798.0
23		399.4	1123.4	40%	1064.0
24		299.8	843.1	50%	1330.0



(a) 5-10mm

(a) 10-25mm

**Fig. 10.** Rounded gravel.

frustum-shaped specimens with the bottom diameter, top diameter and height are 175 mm, 185 mm and 150 mm are casted. After demolding, these specimens are cured at 20°C with relative humidity higher than 95% for 28 days.

#### 4.2. Test of concrete water permeability

The test of concrete permeability are conducted according to the Chinese Standard GB/T 50082-2009 [25]. To begin with, the lateral surface of specimens ought to be wrapped by impervious materials and put into a steel mold. Then, the specimen and steel mold are mounted on the permeation test apparatus (see Fig. 11), which is able to provide a steady water pressure of 0–4.0 MPa. Test configuration is shown in Fig. 12, using permeation test apparatus, the specimen is subjected to a water pressure of 1.2 MPa on its bottom, while the lateral side and top are set as impervious boundary and free boundary exposed to atmospheric pressure, respectively. The action of water pressure lasts 6 h, after which the specimens are demolded and split into two halves so

that the depth of water permeation can be measured. Finally, based on Darcy's Law (vide Eq. (8)) [2,45], the equation deriving the coefficient of concrete permeability can be written as follows:

$$K = \frac{mD_m^2}{2tH} \quad (11)$$

In which  $K(LT^{-1})$  is the coefficient of permeability;  $m$  is the porosity of concrete, generally estimated as 0.03;  $D_m(L)$  is the depth of water permeation;  $t(T)$  is the duration of water pressure, which is 24 h in this experiment;  $H(L)$  is the length of flow path, which is the height of specimen, i.e. 0.15 m.

As aforementioned experimental research has summed up [9], the permeation test is often failed due to improper surface sealing on the lateral side of specimen and high water pressure. In order to solve this problem, after several pre-tests, a two-layer surface sealing consisting of an elastic sheet and a mix of hot paraffin and rosin is adopted (see Fig. 13). By this way, the lateral surface of specimen is much more impervious and able to ensure a more even permeation front. The permeation front of effective and ineffective surface sealing are shown in Fig. 14.

#### 4.3. Experimental phenomenon

Taking 6 specimens whose w/c ratio equal to 0.3 and 0.5 as example, different permeation fronts of concrete with different w/c ratios and aggregate volume fractions are shown in Fig. 15. For the specimen whose w/c ratio = 0.5, as the aggregate volume fraction increase, the permeation depth keeps shrinking and the permeation front become more and more uneven, which is mainly because the inclusion of low-permeability aggregate. While for the specimen set whose w/c ration = 0.3, only a little change in permeation front can be seen. Therefore, the effects of aggregate on water permeability of concrete with different w/c ratios varies from each other.

#### 4.4. Experimental results

Using the experimental data of permeation depth, based on Eq. (1), the water permeability coefficient of each concrete specimen can be calculated. By averaging the water permeability coefficient of each concrete mix proportion, the water permeability coefficient corresponding to each mix proportion is derived, as is shown in Fig. 16. From the experimental results, we can see that as the increase of w/c ratio, the permeability of concrete increase rapidly.



Fig. 11. Permeation test apparatus.

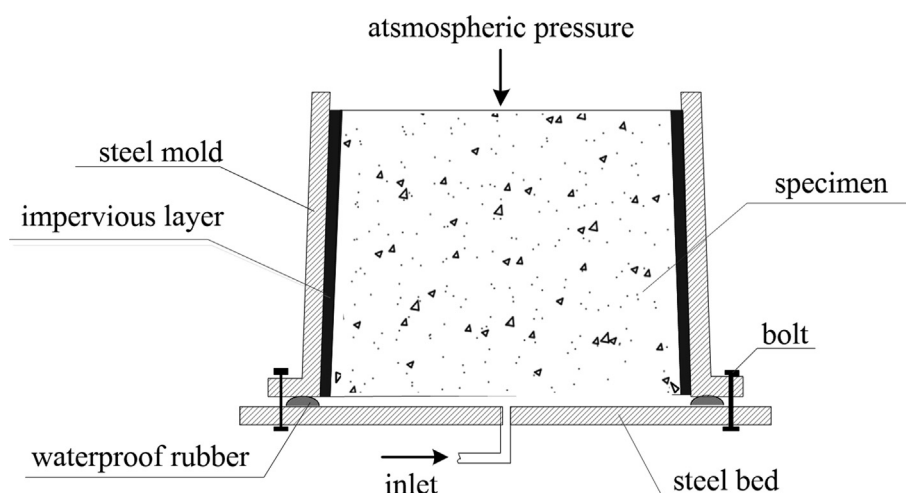
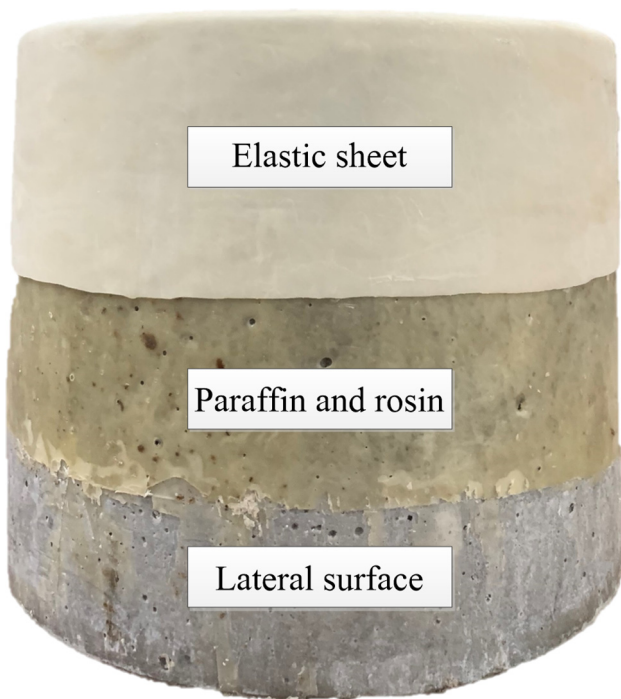


Fig. 12. Test configuration.



**Fig. 13.** Two-layer surface sealing.

Furthermore, the larger the w/c ratio is, the increasing rate of concrete water permeability get faster, which is consistent with the previous studies [5–9]. For concrete specimen of different w/c ratio, aggregate play a different role in affecting the overall concrete water permeability. When the w/c ratio is between 0.4 and 0.6, the concrete water permeability decreases differently as the aggregate volume fraction increase. The bigger w/c ratio is, the faster the concrete water permeability decreases as the increase of aggregate volume fraction. While when the w/c ratio is 0.3, little fluctuation of concrete water permeability can be seen with the change of aggregate volume fraction. Overall, the volume fraction of aggregate influence water permeability of concrete in different extent, depending on the w/c ratio of the concrete, which, in other words, is the strong indication of the water permeability of mortar.

In order to investigate how aggregate can influence the concrete water permeability, we take the effectiveness factor of concrete water permeability  $\eta$  as the main target to analyze further. As is shown in Fig. 17, for concrete specimen whose w/c ratio is 0.4 ~ 0.6, the value of  $\eta$  decreases as the increase of the aggregate

volume fraction, and the bigger the w/c ratio is, the faster  $\eta$  decreases, which shows the same pattern revealed in Fig. 16, indicating that aggregate have a more significant impact on reducing the concrete water permeability when concrete is of bigger w/c ratio. While for concrete specimen whose w/c ratio equals 0.3, a clearer upward trend of  $\eta$  can be seen compared to that in Fig. 17, where the water permeability of concrete seems to remain unchanged as the increase of aggregate volume fraction.

From the experimental results, we can infer that when the concrete is of relatively higher w/c ratio (0.4 ~ 0.6), the cement mortar possesses higher water permeability than that of aggregate. Therefore, it's understandable that the ingress of less permeable aggregate can reduce the overall water permeability of concrete, which is consistent with most of the previous studies [14–24]. While when the w/c ratio is relatively lower (0.3), the mortar may become even less permeable than aggregate so that the more aggregates are mixed in concrete, the more permeable the concrete is. Based on the experimental results, we can see that the value of aggregate water permeability is between that of mortar whose w/c ratio are 0.3 and 0.4, respectively.

## 5. Results and discussion

### 5.1. The effect of aggregate permeability on concrete water permeability

In order to determine the relatively exact value of aggregate water permeability coefficient (represented by  $k_a$ ), based on the meso-structure of concrete specimen with aggregate volume fraction ranging from 10% to 50% and the  $k_a/k_m$  ratio varying from 0.001 to 100000, 35 sets of corresponding effectiveness factors of concrete water permeability (represented by  $\eta$ ) are calculated. On the precondition that the property of ITZ is fixed, the specific value of  $k_m$  has little influence on the value of  $\eta$ , since it represents the slope ratio of  $k_{eff}$ - $k_m$  curve, as is shown in Fig. 9. Note that for different mortar permeability ( $k_m$ ), the permeability of ITZ ( $k_i$ ) can be different because both cement mortar permeability ( $k_m$ ) and the formation of ITZ are strongly affected by w/c ratios and curing conditions. Therefore during the process of estimating  $k_a$ , the w/c ratio is fixed to be 0.5. Accordingly, the value of  $k_m$  here is  $6.612 \times 10^{-12} \text{ m/s}$ .

The influences of aggregate permeability on the concrete water permeability can be seen in Fig. 18. The red dash line represents for the upper or lower limits of  $k_a/k_m$  ratio, beyond which the value of  $\eta$  will converge to a constant value with fluctuation range smaller than 1.0%. And the green dash line denotes the ultimate value of  $\eta$  when  $k_a/k_m$  ratio exceeds the upper or lower limits represented by

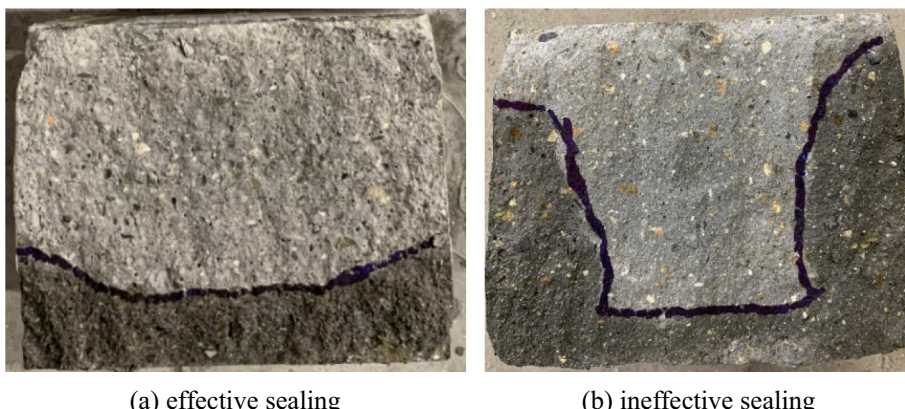


**Fig. 14.** Effects of surface sealing on concrete permeation front.

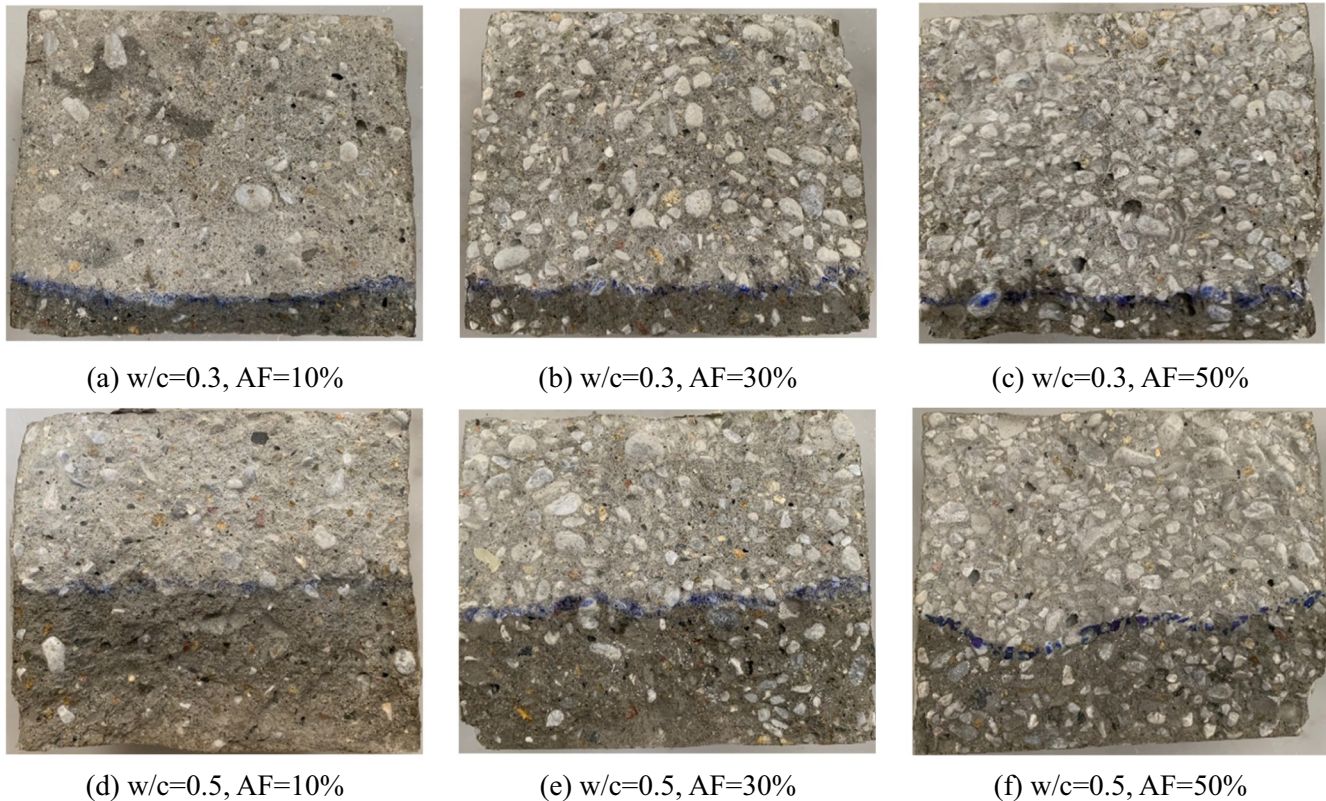


**Fig. 15.** The permeation front of some specimens. (Note that "AF" represents for "aggregate volume fraction").

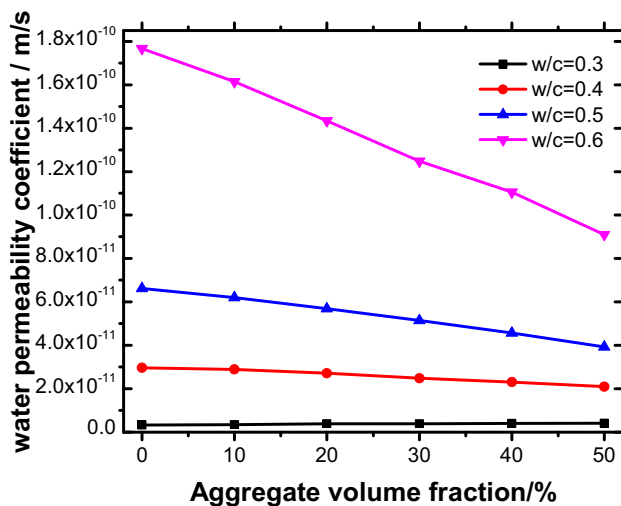


**Fig. 16.** The experimental results of concrete water permeability with different w/c ratio and aggregate fraction.

red dash line. When the value of  $k_a/k_m$  ratio is between the lower and upper limit represented by red dash line, a little fluctuation of  $k_a/k_m$  ratio can result in large change on the value of  $\eta$ , so a more precise value of  $\eta$  requires a more exact value of  $k_a$ . While when the value of  $k_a/k_m$  ratio is beyond the lower or upper limit, the fluctuating range of  $\eta$  is restricted within 1%, which means that the exact value of aggregate permeability makes little difference on  $\eta$ . Hereby, the region between the lower and upper limit can be defined as a Sensitive Zone, in which the value of  $\eta$  is highly sensitive to  $k_a$ .

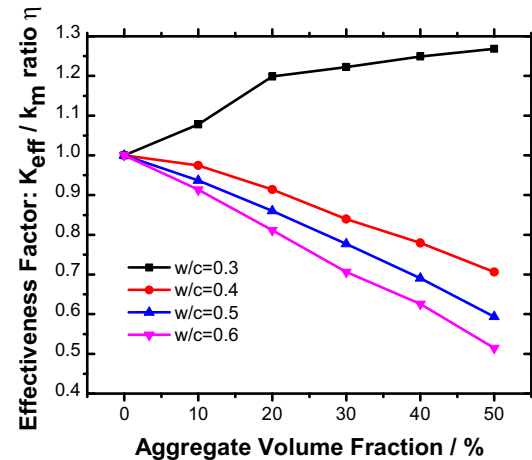


**Fig. 17.** The experimental results of  $k_{eff}/k_m$  with different w/c ratio and aggregate fraction.

As is shown in Fig. 18, as the  $k_a/k_m$  ratio increases,  $k_{eff}/k_m$  ratio keeps rising. However, the increasing rate shows significant difference at different stage. When  $k_a/k_m > 1$  (i.e.  $\log(k_a/k_m) > 0$ ), the  $k_{eff}/k_m$  ratio grows more rapidly, which indicates that if the aggregate is more permeable than the mortar (e.g. concrete using recycled aggregate or High Strength Concrete with very low w/c ratio), the inclusion of aggregate can exert much greater influence on the permeability of concrete. More importantly, the  $\eta$ - $\log(k_a/k_m)$  curve illustrates that if the value of  $k_a/k_m$  is within the Sensitive Zone, then the assumption that aggregate is permeable or impermeable is unpractical, and an exact value of  $k_a$  is required to ensure necessary precision of numerical results. Furthermore, as the

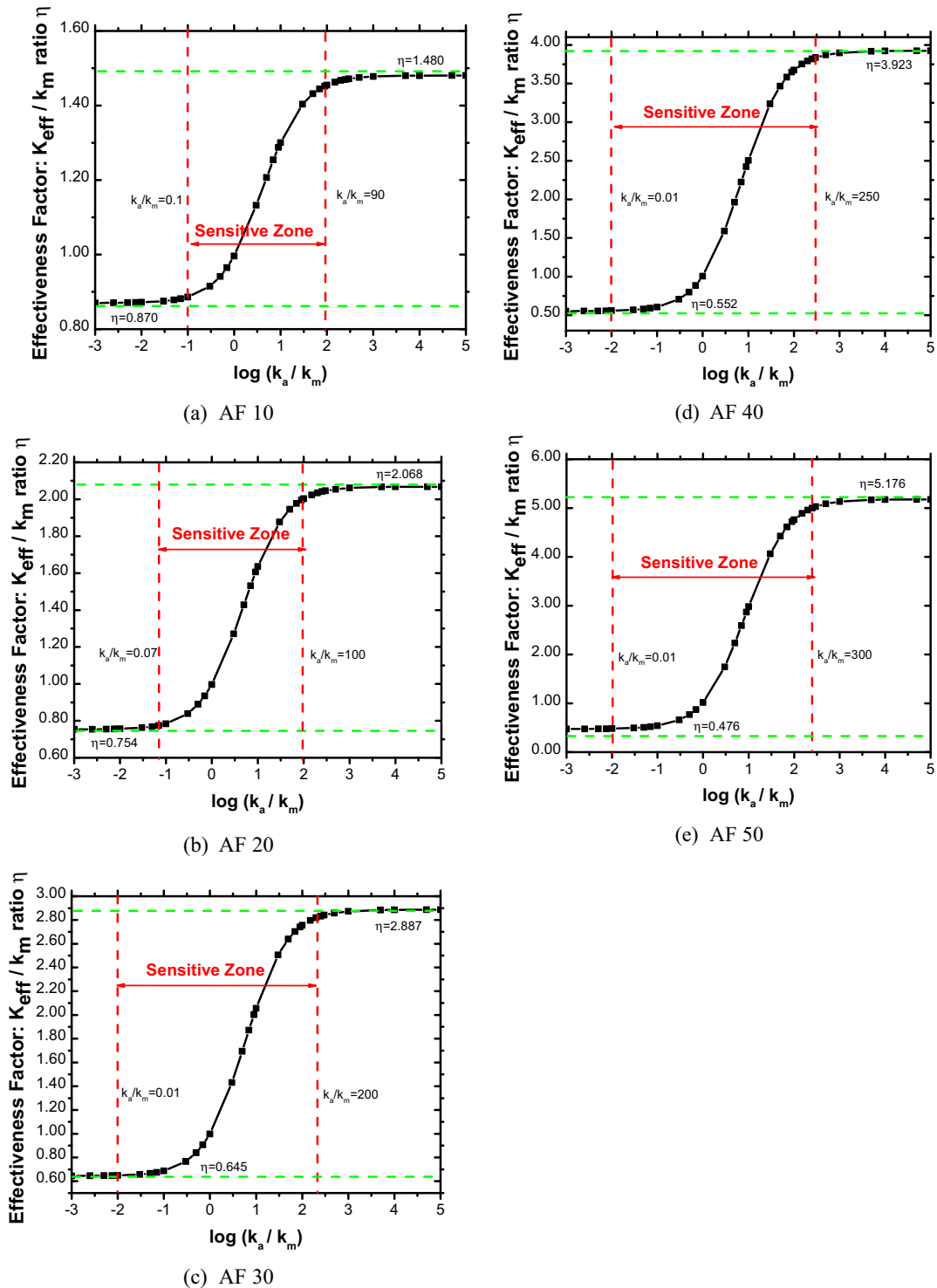


**Fig. 18.** Numerical results of different  $k_{eff}/k_m$  ratios for different  $ka/km$  (Note that "AF" represents for "aggregate volume fraction").

increase of aggregate volume fraction, the width of sensitive zone gets larger, meaning that the calculating precision of concrete water permeability with higher aggregate fraction are more likely to depend on the exact value of  $k_a$ .

### 5.2. The estimation of aggregate water permeability

Based on the  $\eta$ - $\log (k_a/k_m)$  curve and experimental results, linear interpolation is performed to estimate the aggregate water

permeability ( $k_a$ ). **Table 2** shows the process of how the estimated value of  $k_a$  is derived. According to the experimental results (shown in **Fig. 16**), when the w/c ratio is 0.5, the  $k_{eff}/k_m$  ratio of concrete specimen whose aggregate volume fraction is 10%, 20%, 30%, 40%, 50% is 0.93, 0.86, 0.78, 0.70, 0.63, respectively. Furthermore, by performing linear interpolation on the  $k_{eff}/k_m - \log (k_a/k_m)$  curve in **Fig. 18**, the  $k_a/k_m$  ratio that corresponds to  $k_{eff}/k_m$  mentioned above is 0.402, 0.371, 0.331, 0.282, 0.233, respectively. Based on experimental results of mortar permeability

**Table 2**The calculation table of estimated  $k_a$ .

Aggregate Volume Fraction	10%	20%	30%	40%	50%
$k_{eff}/k_m$ ratio (experiment)	0.93	0.86	0.78	0.70	0.63
$k_a/k_m$ ratio (interpolation)	0.402	0.371	0.331	0.282	0.233
$k_a$ (estimation) (Unit: m/s)	$2.658 \times 10^{-12}$	$2.453 \times 10^{-12}$	$2.189 \times 10^{-12}$	$1.865 \times 10^{-12}$	$1.541 \times 10^{-12}$
Relative deviation	24.15%	14.58%	2.22%	-12.91%	-28.04%
Averaged $k_a$ (Unit: m/s)	$2.141 \times 10^{-12}$				

(also shown in Fig. 16), the estimated value of  $k_a$  of each w/c ratio is derived. As we can see in Table 2, by this way, the value of  $k_a$  we calculated contains certain errors, which are probably resulted from the experiments and assumed parameters of ITZ. Finally, by averaging the values of  $k_a$  of different w/c ratios, the final estimated  $k_a$  is  $2.141 \times 10^{-12}$  m/s.

### 5.3. The verification of numerical modeling

Fig. 19 shows the numerical and experimental results of how water permeability of concrete with different w/c ratios change with the increase of aggregate volume fraction. The numerical

results illustrated here are based on both models with the estimated  $k_a$  and the assumption that aggregate is impermeable (i.e.  $k_a = k_m \times 10^{-5}$ ). Because of the inherent heterogeneity of concrete and inevitable visual error which is likely to happen in the measurement of permeation depth of concrete specimen, the experimental data shows obvious discreteness. Especially when the value of w/c ratio is smaller, the fluctuation range of experimental data gets relatively bigger, which is mainly because when w/c ratio is small, the value of water permeability is also relatively small, and from Eq. (1) we can see that even a small change happened to the permeation depth can result in big fluctuation in the value permeability coefficient.

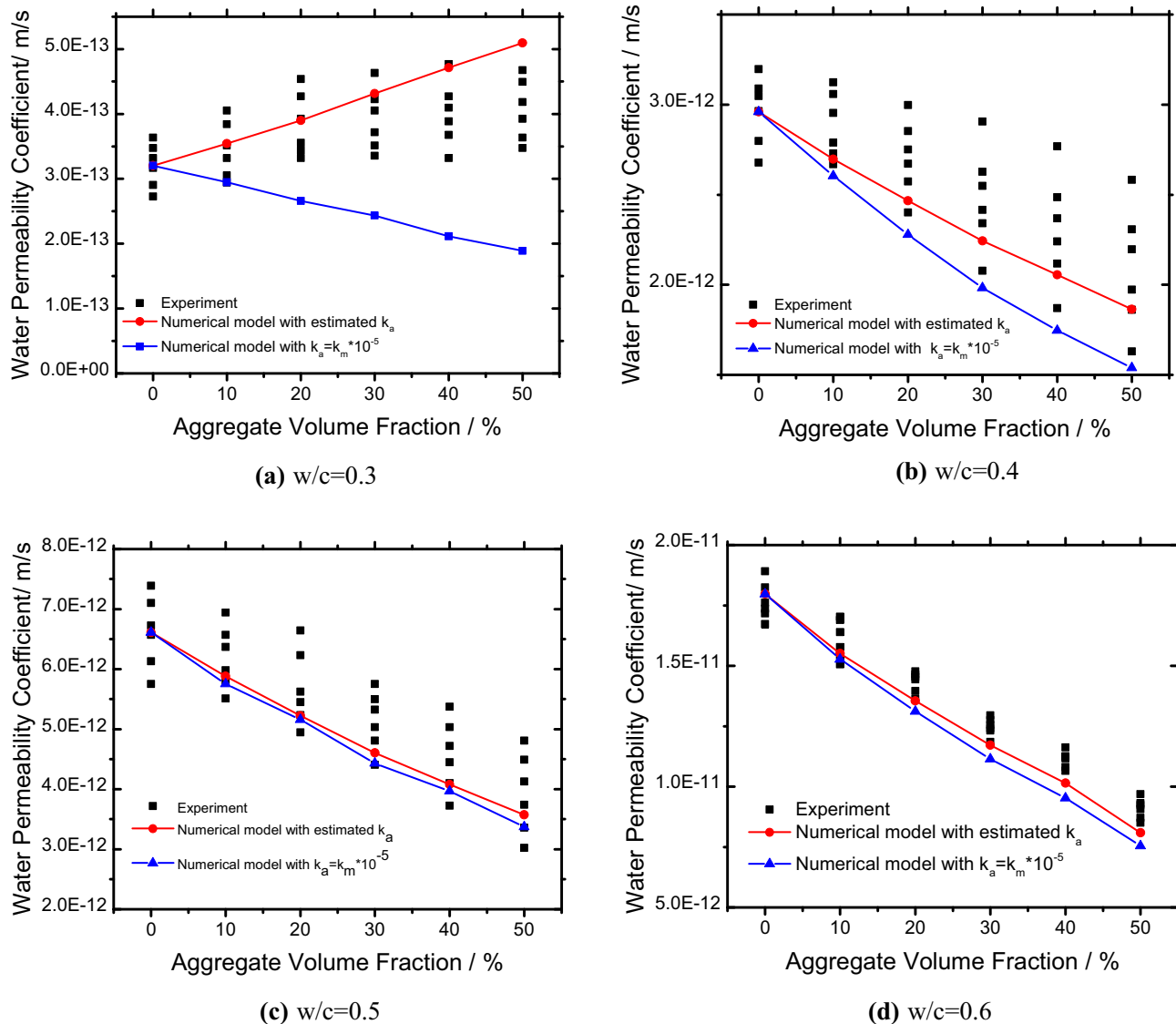


Fig. 19. The comparison between the numerical and experimental results.

By comparing the experimental and numerical results with estimated  $k_a$ , we can see that under different w/c ratios, concrete water permeability changes with aggregate volume fraction similarly in both experiments and numerical models with estimated  $k_a$ . However, because  $k_a$  is estimated by the numerical modeling and experimental results, and the thickness and permeability coefficient of ITZ are obtained directly from relative previous studies, there are still some differences between the magnitude of numerical and experimental results. When w/c ratio is 0.3, as the increase of aggregate volume fraction, the numerical values are gradually becoming bigger than that of experimental values. While when w/c ratio is 0.4 ~ 0.6, as the increase of aggregate volume fraction, the numerical values are gradually becoming smaller than that of experimental values. The difference of experimental results and numerical results with estimated  $k_a$  may mainly resulted from the assuming ITZ parameters and non-thickness geometry.

When the aggregate permeability is overlooked and the value of  $k_a$  is set to be  $10^{-5}$  times of  $k_m$ , different trends of how water permeability changes with aggregate volume fraction can be seen in concrete of different w/c ratios. As is shown in Fig. 19, as the increase of w/c ratio from 0.3 to 0.6, the gap between experimental results and numerical results with  $k_a = k_m \times 10^{-5}$  keeps shrinking. When w/c ratio is low (i.e. w/c = 0.3), the numerical results with  $k_a = k_m \times 10^{-5}$  show a totally opposite trend with the experiment, while when w/c ratio reaches 0.5, a much reliable and precise results can be seen. Such differences indicate that when w/c ratio is lower than 0.4, the value of  $k_a/k_m$  is located within Sensitive Zone (shown in Fig. 18), in which the exact value of  $k_a$  exerts significant influence on the precision of numerical results.

In order to further compare the results of two numerical models, the Mean Relative Error (MRE) of both numerical models and Mean Relative Standard Deviation (MRSD) of experimental results are calculated according to Eq. (11):

$$MRE = \frac{1}{5} \sum_{n=1}^5 \frac{K_{num,n} - K_{exp,n}}{K_{exp,n}} \quad (11a)$$

$$MRSD = \frac{1}{5} \sum_{n=1}^5 \frac{s_{exp,n}}{K_{exp,n}} \quad (11b)$$

where  $n = 1 \sim 5$  denotes the results of concrete with aggregate volume fraction ranging from 10% to 50%;  $K_{num,n}$  represents for the numerical results of concrete water permeability;  $K_{exp,n}$ ,  $s_{exp,n}$  is the average and standard deviation of six experimental results of concrete with certain w/c ratio and aggregate volume fraction. For example,  $K_{num,3}$  represents the concrete water permeability coefficient calculated by numerical model with aggregate volume fraction equals 30%. The results of MRE can be seen in Table 3.

As is shown in Table 3, with the incorporation of estimated  $k_a$ , the precision of numerical results sees significant improvement when compared with results of models which assume the aggregate as impermeable and directly set  $k_a = k_m \times 10^{-5}$ . The MRSD of experiment (around 12%) can be seen as an ideal error that is totally acceptable in numerical results. As all the MRE of numerical results with estimated  $k_a$  can be restricted within 12%, the estimation of  $k_a$  and further numerical results is verified. While on the

other hand, when w/c ratio reaches 0.5, MRE of numerical results with  $k_a = k_m \times 10^{-5}$  can also be within 12%. This fact indicates that when w/c ratios possess a higher value (i.e. cement mortar is much permeable.), it's safe to presume aggregate as impermeable in numerical models, but the precision of such models is still expected to be lower than models with more suitable value of  $k_a$ .

## 6. Conclusions

This paper presents an efficient method to establish sophisticated 3D three-phase meso-scale model of concrete, which is used to investigate concrete water permeability. Meanwhile, a series of permeation tests of concrete containing one kind of aggregate and different w/c ratios are carried out to provide parameters and verification for numerical models. Through numerical modeling and the analysis of experiments, some important conclusions can be drawn as follows:

- 1) The meso-scale model of concrete composed of ellipsoidal aggregate, non-thickness ITZ and homogeneous matrix is able to reflect the effects of tortuosity, dilution and ITZ, which are resulted from the random ingress of coarse aggregates reasonably.
- 2) The Node Local Density-Oriented Method proposed in this paper can promote the efficiency of generating random ellipsoidal aggregate structure, which can be further used to investigate various properties of concrete on meso-scale.
- 3) For a given aggregate volume fraction and certain ITZ parameters, the concrete water permeability ( $K_{eff}$ ) is approximately directly proportional to cement mortar permeability ( $k_m$ ), and the slope of  $K_{eff} - k_m$  curve represent the effectiveness factor of concrete water permeability ( $\eta$ ).
- 4) The assumption that aggregate is impermeable can cause apparent errors of numerical results when the value of  $k_a/k_m$  is located within Sensitive Zone ( $k_a/k_m = 0.07 \sim 300$ ). While when  $k_a/k_m$  is outside of Sensitive Zone, concrete water permeability will converge to a constant value not matter what value is assigned to  $k_a$ .
- 5) The estimation of aggregate permeability can significantly improve the precision of numerical models for concrete water permeability. When w/c ratio of concrete is low (w/c < 0.4), it's necessary to provide a more suitable value of aggregate permeability to ensure necessary precision. While when w/c ratio of concrete is high (w/c > 0.5), the model based on assumption of impermeable aggregate can also derive numerical results of acceptable precision.

## CRediT authorship contribution statement

**Minfei Liang:** Conceptualization, Methodology, Software, Investigation, Writing - original draft, Writing - review & editing. **Kun Feng:** Conceptualization, Methodology, Writing - review & editing, Supervision. **Chuan He:** Conceptualization, Methodology, Supervision, Resources. **Yuqiang Li:** Software, Validation, Investigation. **Lin An:** Conceptualization, Methodology. **Wenqi Guo:** Data curation, Investigation.

**Table 3**  
MRSD of experiments and MRE of numerical models.

W/C ratio	0.3	0.4	0.5	0.6
MRSD of experiment	12.36%	11.02%	11.97%	4.05%
MRE of model with estimated $k_a$	11.47%	-9.40%	-8.66%	-7.00%
MRE of model with $k_a = k_m \times 10^{-5}$	-36.78%	-19.32%	-11.48%	-11.11%

## Declaration of Competing Interest

The authors declare that they have no known competing financial interests or personal relationships that could have appeared to influence the work reported in this paper.

## Acknowledgment

The authors appreciate the support of the National Natural Science Foundation of China (Grant No. 51878569, No. 51578462).

## References

- [1] C. Hall, W.D. Hoff, *Water Transport in Brick, Stone and Concrete*, Spon Press, London, 2012.
- [2] L. Basheer, J. Kropp, D.J. Cleland, Assessment of the durability of concrete from its permeation properties: a review, *Constr. Build. Mater.* 15 (2001) 93–103.
- [3] H.W. Reinhardt, Penetration and permeability of concrete: barriers to organic and contaminating liquids, *RILEM Report 16*, E&FN Spon, London, 1997.
- [4] A.M. Neville, *Properties of Concrete*, Edition Eyrolles, fourth ed., Longman Group Limited, England, 2000.
- [5] C. Thomas, J. Setién, J.A. Polanco, et al., Durability of recycled aggregate concrete, *Constr. Build. Mater.* 40 (2013) 1054–1065.
- [6] A.K. Jain, J.S. Chouhan, Effect of Shape of aggregate on compressive strength and permeability properties of pervious concrete, *Int. J. Adv. Eng. Res. Stud.* 1 (2011) 120–126.
- [7] W.A.R.D.A. Bint Ashraf, M.A. Noor, Effects of aggregate gradation on water permeability of concrete, *Adv. Mater. Res.* 488–489 (2012) 248–252.
- [8] X. Liu, K.S. Chi, M.-H. Zhang, Water absorption, permeability, and resistance to chloride-ion penetration of lightweight aggregate concrete, *Constr. Build. Mater.* 25 (2011) 335–343.
- [9] A. Amriou, M. Bencheikh, New experimental method for evaluating the water permeability of concrete by a lateral flow procedure on a hollow cylindrical test piece, *Constr. Build. Mater.* 151 (2017) 642–649.
- [10] K.S. Chia, M.-H. Zhang, Water permeability and chloride penetrability of high-strength lightweight aggregate concrete, *Cem. Concr. Res.* 32 (2002) 639–645.
- [11] K. Čosić, L. Korat, V. Ducman, I. Netinger, Influence of aggregate type and size on properties of pervious concrete, *Constr. Build. Mater.* 78 (2015) 69–76.
- [12] A. Perrot, D. Rangeard, V. Picandet, S. Serhal, Effect of coarse particle volume fraction on the hydraulic conductivity of fresh cement based material, *Mater. Struct.* 7 (2014) 2291–2297.
- [13] Ha-Won Song, Seung-Woo Pack, Sang-Hyeok Nam, et al., Estimation of the permeability of silica fume cement concrete, *Constr. Build. Mater.* 24 (2010) 315–321.
- [14] Du Xiuli, Liu Jin, Guowei Ma, A meso-scale numerical method for the simulation of chloride diffusivity in concrete, *Finite Elem. Anal. Des.* 85 (2014) 87–100.
- [15] Qing-feng Liu, Gan-lin Feng, Jin Xia, Jian Yang, Long-yuan Li, Ionic transport features in concrete composites containing various shaped aggregates: a numerical study, *Compos. Struct.* 183 (2018) 371–380.
- [16] Jianjun Zheng, Xinzhu Zhou, Xiaofeng Huang, Fu. Chuanqing, Experiment and modeling of the effect of aggregate shape on the chloride diffusivity of concrete, *J. Mater. Civ. Eng.* 26 (9) (2014) 04014048.
- [17] S.D. Abayneh, H.S. Wong, N.R. Buenfeld, Modelling the diffusivity of mortar and concrete using a three-dimensional mesostructure with several aggregate shapes, *Comput. Mater. Sci.* 78 (2013) 63–73.
- [18] Yuanzhan Wang, Wu. Linjian, Yuchi Wang, Effects of coarse aggregates on chloride diffusion coefficients of concrete and interfacial transition zone under experimental drying-wetting cycles, *Constr. Build. Mater.* 185 (2018) 230–245.
- [19] Wu Jie, Jean-Baptiste Mawulé Dasseko, Chengyong Wan, et al., Experimental and numerical modeling of chloride diffusivity in hardened cement concrete considering the aggregate shapes and exposure-duration effects, *Results Phys.* 7 (2017) 1427–1432.
- [20] C.S. Zhou, K.F. Li, Numerical and statistical analysis of permeability of concrete as a random heterogeneous composite, *Comput. Concr.* 7 (5) (2010) 469–482.
- [21] D.J. Manuka Wimalasiri, Chun-Qing Li Robert, A new method to simulate permeability degradation of stressed concrete, *Constr. Build. Mater.* 174 (2018) 284–292.
- [22] Xinxin Li, Xu. Yi, Shenghong Chen, Computational homogenization of effective permeability in three-phase mesoscale concrete, *Constr. Build. Mater.* 121 (2016) 100–111.
- [23] Xinxin Li, Xu. Qing, Shenghong Chen, An experimental and numerical study on water permeability of concrete, *Constr. Build. Mater.* 105 (2016) 503–510.
- [24] Chun-Qing Li, Hassan Baji, Shangtong Yang, Probabilistic study on hydraulic conductivity of concrete at mesoscale, *ACI Mater. J.* 115 (2018) 717–725.
- [25] W.F. Brace, J.B. Walsh, W.T. Frangos, Permeability of granite under high pressure, *J. Geophys. Res.* 73 (6) (1968) 2225–2236.
- [26] C.E. Neuzil, C. Cooley, S.E. Silliman, J.D. Bredehoeft, P.A. Hsieh, A transient laboratory method for determining the hydraulic properties of 'Tight' Rocks e II. Application, *Int. J. Rock Mech. Mining Sci. Geomech. Abstracts* 18 (3) (1981) 253–258.
- [27] S. Escoffier, F. Homand, A. Giraud, N. Hoteit, K. Su, Under stress permeability determination of the Meuse/Haute-Marne mudstone, *Eng. Geol.* 81 (3) (2005) 329–340.
- [28] A.P.S. Selvadurai, L. Jenner, Radial flow permeability testing of an argillaceous limestone, *Groundwater* 51 (1) (2013) 100–107.
- [29] Z.J. Pan, Y. Ma, L.D. Connell, D.I. Down, M. Camilleri, Measuring anisotropic permeability using a cubic shale sample in a triaxial cell, *J. Nat. Gas Sci. Eng.* 26 (2015) 336–344.
- [30] V.I. Malkovsky, A.V. Zharikov, V.M. Shmonov, New methods for measuring the permeability of rock samples for a single-phase fluid, *Phys. Solid Earth.* (45) (2009) 89–100.
- [31] T.C. Powers, Structure and physical properties of hardened Portland cement paste, *J. Am. Ceram. Soc.* 41 (1958) 1–6.
- [32] T.C. Powers, L.E. Copeland, J.C. Hayes, H.M. Mann, Permeability of Portland cement paste, *J. Am. Concr. Inst.* 51 (1954) 285–298.
- [33] W.B. Fuller, S.E. Thompson, The laws of proportioning concrete, *Trans. Am. Soc. Civil Eng.* 59 (2) (1907) 67–143.
- [34] S.T. Erdogan, D.W. Fowler, Determination of Aggregate Shaper Properties Using X-Ray Tomographic Methods and the Effect of Shape on Concrete Rheology, The University of Texas at Austin, Austin, 2005.
- [35] Wenping Wang, Jiaye Wang, Myung-Soo Kim, An algebraic condition for the separation of two ellipsoids, *Comput. Aided Geom. Des.* 18 (2001) 531–539.
- [36] P. Wriggers, S.O. Moftah, Mesoscale models for concrete: homogenisation and damage behavior, *Finite Elem. Anal. Des.* 42 (7) (2006) 623–636.
- [37] H.F. Ma, H.Q. Chen, B.K. Li, Influence of meso-structure heterogeneity on bending strength of concrete, *J. Hydraulic Eng.* 36 (2005) 846–852.
- [38] COMSOL Multiphysics User's Guide, Version 5.4. COMSOL Inc, Burlington, Massachusetts, USA, 2018, [www.comsol.com](http://www.comsol.com).
- [39] K.M. Nemati, P. Gardoni, Microstructural and statistical evaluation of interfacial zone percolation in concrete, in: 11th International Conference on Fracture (ICF11), 2005, pp. 191–197.
- [40] D.N. Winslow, M.D. Cohen, D.P. Bentz, K.A. Snyder, E.J. Garboczi, Percolation and pore structure in mortars and concrete, *Cem. Concr. Res.* 24 (1994) 25–37.
- [41] J. Ollivier, J. Maso, B. Bourdette, Interfacial transition zone in concrete, *Adv. Cement Base Mater.* 2 (1) (1995) 30–38.
- [42] K.L. Scrivener, A.K. Crumble, P. Laugesen, The interfacial transition zone (ITZ) between cement paste and aggregate in concrete, *Interface Sci.* 12 (2004) 411–421.
- [43] J.D. Shane, T.O. Mason, H.M. Jennings, et al., Effect of the interfacial transition zone on the conductivity of Portland cement mortars, *J. Am. Ceram. Soc.* 83 (2000) 1137–1144.
- [44] Kai Li, Piet Stroeven, Martijn Stroeven, et al., A numerical investigation into the influence of the interfacial transition zone on the permeability of partially saturated cement paste between aggregate surfaces, *Cement Concr. Res.*, 102 (2017) 99–108.
- [45] GB/T 50082-2009, Standard for test methods of long-term performance and durability of ordinary concrete, China Architecture & Building Press, Beijing, 2009.